JGR Solid Earth

Key Points:

- Both high-Ti and low-Ti picrites in the Emeishan large igneous province are hydrous
- The major and trace element compositions of picrites are related to the water content in their mantle sources
- Compositional variations in a large igneous provinces are affected by volatiles in mantle plumes

Supporting Information:

Supporting Information may be found in the online version of this article.

Compositional Variation of Picrites in the Emeishan Large Igneous Province Modulated by Water in the Mantle Plume

J. Liu[1] , **Q. K. Xia[1]** , **H. Sun[1]**, **E. Hanski[2]**, **T. Kuritani[3]**, **X. Y. Gu[1]** , and **H. Chen[1]**

[1]School of Earth Sciences, Key Laboratory of Geoscience Big Data and Deep Resource of Zhejiang Province, Zhejiang University, Hangzhou, China, [2]Oulu Mining School, University of Oulu, Oulu, Finland, [3]Graduate School of Science, Hokkaido University, Sapporo, Japan

Abstract Initiation of large igneous provinces (LIPs) and temporal and spatial variations in their chemical compositions provide unique opportunities to understand mantle dynamics. It has been recently revealed that water-rich reservoirs in the mantle sources have played a significant role in the production of LIPs. However, the dominant causes for the chemical variations in primitive magmas of LIPs remain debated. In the Emeishan LIP (ELIP), there are several places where picrites accompany more abundant flood basalts. These picrites span a large range of Ti/Y, Sm/Yb, and TiO_2/Al_2O_3. In this work, we have determined the water contents of picrites with Ti/Y > 500 from the ELIP, based on the water content of clinopyroxene phenocrysts and water partitioning coefficients. We have also calculated the water content of the mantle sources by applying batch and fractional partial melting models. We show that the chemical compositions of picrites in the ELIP closely correlate with the calculated water content in their mantle sources. Our model suggests that the variation in the chemical composition of the primary magmas of the ELIP both on a local and regional scale can be mainly explained by the complementary roles of relatively dry recycled pyroxenite and hydrated components in the mantle plume, without requiring catastrophic thinning of the lithospheric mantle. Our model thus implies that both the initiation and chemical variation of the ELIP are affected by water from the deep mantle.

Plain Language Summary Large igneous provinces (LIPs) represent a manifestation of the activity of a mantle plume. In most LIPs, the chemical compositions of basalts are heterogeneous and can usually be divided into high-Ti and low-Ti groups. This division has been used to infer differences in the mantle composition and/or partial melting conditions, which ultimately reflect the picture of the compositional and thermal structure of the deep mantle and their partial melting processes. In this study, we report that both the high-Ti and low-Ti type picrites of the Emeishan LIP were derived from hydrous mantle sources and such a compositional dichotomy is closely associated with the water content of the mantle sources. This case study provides a new perspective to connect the presence of volatiles in the deep mantle, the activity of deep-seated mantle plumes, and widespread basaltic magmatism on the Earth's surface.

1. Introduction

Large igneous provinces (LIPs) consist mainly of basaltic rocks erupted rapidly (mostly within 1–5 Ma) over great areas ($0.1–10 \times 10^6$ km^2; Ernst, 2014). Many of them have contributed to the formation of giant metallic ore deposits and triggered prominent environmental effects (Ernst, 2014). The long-recognized characteristics of the global LIPs include the occurrences of low-Ti and high-Ti magmas on local and regional scales (Bryan & Ernst, 2008; Cox et al., 1967), although in specific LIPs, different magma types derived from different sources can exist (Luttinen, 2018). The temporal and spatial occurrence of the high-Ti and low-Ti magma types within volcanic sequences provides a unique window to trace the dynamics of mantle convection and the chemical heterogeneity of the Earth's interior. Paleogeographic reconstructions show that most of the LIPs in the past 300 Ma formed at the edge of large low-shear-wave-velocity provinces (LLSVPs) with thermal and chemical heterogeneities in the lower mantle, which suggests a close genetic relationship between LIPs and mantle plumes (Burke et al., 2008; Torsvik et al., 2010). Many studies have revealed that hydrous reservoirs (with water contents of >2,000 ppm, i.e., much higher than in the mid-ocean ridge basalt and ocean island basalt sources; Hirschmann, 2006) derived from the deep mantle have played a significant role in the initiation of some Archean and Phanerozoic LIPs (Gurenko et al., 2016; Ivanov et al., 2018; Liu et al., 2017; Shimizu et al., 2001; Sobolev et al., 2016).

Although varying degrees of differentiation and lithospheric contamination have played a significant role in the compositional variations of many eruptive sequences in continental LIPs (Ernst, 2014; Hawkesworth et al., 1995; Jourdan et al., 2007; Luttinen, 2018), the dominant causes for the compositional variations of more primitive magmas, such as picrites, are still under debate. According to the scenario that mantle plumes are derived from a dry and heterogeneous thermochemical pile, the temporal variation in the chemical composition of primary magmas (e.g., increasing Sm/Yb and Ti/Y ratios with time) have been attributed to a change in the degree of partial melting (Lassiter & DePaolo, 1997) or the relative proportion of recycled-eclogite/pyroxenite-derived melts (Sobolev et al., 2011), which were finally associated with thinning of the lithosphere caused by the interaction with a mantle plume head. However, such an extent of thinning is not easy to occur within a typical main eruption period (several million years) of LIPs, even if the lithospheric mantle has been weakened by hydration (Wang et al., 2015). Water can have a disproportionally large effect on the partial melting behavior of mantle, thereby contributing to the composition of magmas (e.g., Asimov & Langmuir, 2003; Hirschmann, 2006; Katz et al., 2003). Thus, hydrated components entrained by mantle plumes from the Earth's interior may play an important role in the chemical variation of the surface magmatism in the LIPs. Based on the Ni content or Fe/Mn ratio of olivine phenocrysts, Liu et al. (2017) observed a negative trend between the H_2O/Ce ratio and the proportion of pyroxenite-derived melts in erupted primary magmas for several Phanerozoic LIPs and Archean komatiites (e.g., Emeishan, Siberian, Talimu, Karoo, Columbia River, Abitibi komatiite). However, due to the complex dependence of the Ni content and Fe/Mn ratio of olivine on temperature, pressure, and melt composition (Matzen et al., 2017), this work did not directly indicate whether the composition of the primary melt (e.g., in terms of major elements and Sm/Yb or Ti/Y ratios) is correlated with the water content in the mantle source.

The Emeishan large igneous province (ELIP) is located at the western margin of the Yangtze Craton in southwestern China and was formed within one million years at ca. 260 Ma (Zhong et al., 2014). In the western part of the province, the thickest volcanic succession reaches a thickness of ∼5 km (e.g., Binchuan, Lijiang; Xu et al., 2001; Zhang et al., 2006). There are several places where highly magnesian volcanic rocks occur together with more abundant flood basalts (Dali, Binchuan, Lijiang; Hanski et al., 2010; Zhang et al., 2006; Figure S1), varying in composition from LREE-depleted low-Ti picrites to LREE-enriched high-Ti picrites (Hanski et al., 2010). Liu et al. (2017) concluded that the low-Ti picrites at the bottom of the Binchuan succession in the Dali area were derived from a hydrous (>6,000 ppm) eclogite-bearing mantle plume. Here, we focus on high-Ti picrites from several locations (Binchuan, Yongsheng, Lijiang) of the ELIP and examine the potential correlation between the water content in the mantle source and the geochemical composition of the primary magmas. The new water content data of these rocks suggest that their mantle sources could have >3,000 ppm H_2O, while the calculated olivine liquidus temperatures are comparable to those of low-Ti picrites (∼1,340 °C). We show that the compositions (e.g., Ti/Y and Sm/Yb ratios) of the ELIP picrites are closely correlated with the water contents of their mantle sources. We thus argue that the formation of the ELIP is closely related to the entrapment of a hydrous reservoir in the Earth's interior, and the compositional fluctuations of the surface magmatism associated with the mantle plumes reflect the complementary partial melting behaviors of recycled eclogites/pyroxenites and hydrated components within the mantle plume.

2. Analytical Methods

2.1. Major and Trace Element Analysis of Bulk-Rock Samples

Major and trace element concentrations of bulk-rock samples were determined at ALS Chemex Co., Ltd. (Guangzhou, China). After removal of weathered surfaces, the samples were crushed into small fragments (<0.5 cm in diameter), cleaned with deionized water and ground to 200-mesh powder, and analyzed for loss-on-ignition. Major element compositions were measured by X-ray fluorescence (XRF) on fused glass disks. The precision for element concentrations of >1 wt.% is 1–3% and for element concentrations of <1 wt.%, it is ∼10%. For trace elements, lithium metaborate flux was added to the sample powder, and the mixture was fused at 1,000 °C and dissolved in 100 ml of 4% nitric acid. The powder was then analyzed using a PerkinElmer inductively coupled plasma mass spectrometer (ICP-MS). The precision is generally better than 5% for most trace elements.

2.2. Electron Microprobe Analysis

Chemical compositions of olivine and clinopyroxene phenocrysts (cpx) and spinel inclusions in olivine were measured by a Shizuma 1720-H electron microprobe in the School of Earth Sciences at Zhejiang University, Hangzhou, China. Back-scattered electron images were utilized to check the homogeneity of the phenocrysts. During the quantitative analysis of cpx phenocrysts and spinel inclusions, the operating conditions were the following: 15 kV accelerating voltage, 20 nA beam current, and 1 μm spot size. For olivine, the analytical method described by Sobolev et al. (2007) was used, employing an accelerating voltage of 20 kV, a beam current of 300 nA, and a spot size of 5 μm. Natural minerals and synthetic oxides were used as standards, and a program based on the ZAF procedure was used for all data correction. All the analytical points in cpx phenocrysts were focused on the same areas used for the Fourier Transform Infrared Spectroscopy (FTIR) analyses. The errors of the EPMA data are <5%, except for Na_2O of pyroxene, which may have an error of up to 15–20%.

2.3. Fourier Transform Infrared Spectrometry (FTIR)

Usually the water content in anisotropic minerals should be determined by polarized infrared beam (Libowitzky & Rossman, 1996). However, most clinopyroxene phenocrysts in our samples are small and partly altered and bear cracks and inclusions (Figure S2), which make the use of a polarized beam difficult. Xia et al. (2013) and Liu et al. (2015) confirmed that if a cpx grain shows three groups of OH bands ($\sim$3,640, $\sim$3,540, 3,460 cm^{-1}) and the linear absorption (peak height) is less than 0.3, the water content can be determined by the unpolarized infrared beam method using a single randomly oriented crystal. Recently, the validity of the unpolarized FTIR method has been demonstrated in recovering the primary water content of some ocean island basalts (Turner et al., 2017). In this work, unpolarized infrared spectra were obtained at wavenumbers varying from 1,500 to 4,500 cm^{-1} on a Nicolet FTIR spectrometer IS50 coupled with a Continuμm microscope at Zhejiang University, using a KBr beam-splitter and a liquid-nitrogen cooled MCT-A detector. Double-polished thin sections with thicknesses ranging from 0.12 to 0.15 mm were prepared. The light source and pathway and the sample-holding cell were flushed with purified air free of CO_2 and H_2O. For each cpx grain, a total of 256 scans (depending on the water content of the grain) with a resolution of 4 cm^{-1} were performed. A square light spot with dimensions ranging from 30×30 to 100×100 μm was used, depending on the size and quality of the mineral grain. Optically clean, inclusion-free and crack-free areas were carefully chosen for measurement. Absorption by alteration or fluid inclusions in cracks, generally characterized by the OH bands near 3,670 cm^{-1} or near 3,400 cm^{-1} (Ingrin et al., 1989; Keppler & Rauch, 2000), were excluded. For some large cpx phenocrysts, core-to-rim profile analyses were conducted to evaluate the extent of water diffusion during the ascent of their host magma to the surface. For each sample, olivine phenocrysts were also investigated by FTIR, but no visible structural OH bands were detected.

2.4. Water Content of Primary Melts

Water contents of the picritic melts from which the studied clinopyroxene phenocrysts crystallized were calculated using the method of Liu et al. (2017). First, the water content of cpx grains was calculated by the Beer-Lambert law:

$$C = 3 \times A/(I \times t) \tag{1}$$

where C is the water content of cpx in ppm, A is the unpolarized integral absorbance, I is the absorption coefficient, and t is the thickness in cm. Then, the water partition coefficient ($D_{H2O}^{cpx/melt}$) was calculated on the basis of the major element composition of cpx determined by EPMA and the following equation (O'Leary et al., 2010):

$$\ln D_{H2O}^{cpx/melt} = -4.2 \ (\pm 0.2) + 6.5 \ (\pm 0.5)X_{IV_{Al}}^{cpx} - 1.0 \ (\pm 0.2)X_{Ca}^{cpx} \tag{2}$$

The water content of the melt was calculated using the water content of cpx determined by FTIR and the calculated $D_{H2O}^{cpx/melt}$ value. The water content of the parental magma was recovered from these melt water contents taking into account the effects of fractionation and diffusion as discussed later.

2.5. Crystallization Temperature of Olivine Phenocrysts and Mantle Potential Temperature

The Al-in-olivine thermometer developed by Coogan et al. (2014) is based on the partitioning of Al between coexisting spinel and olivine and is not affected by variation in the melt water content and oxygen fugacity. The temperature uncertainty of this thermometer is estimated to be ± 25 °C. Olivine phenocrysts from Lijiang picrites have lower Fo (85–89 mol.%) compared to Yongsheng and Dali picrites, representing products of a later evolutional stage, which was not taken into account in the calculations. We then use the relationship between the mantle potential temperature (T_p) and the liquidus temperature of primary melt established by Herzberg and Asimow (2015) to calculate the final mantle potential temperature. This approach was also applied by Sobolev et al. (2016) to calculate the mantle potential temperature of Archean komatiites derived from mantle sources with thousands ppm of water. Due to the observations that the Al-in-olivine thermometer is not sensitive to magma water content (Coogan et al., 2014), the liquidus temperature of the primitive magma recovered by this approach is consistent with the results calculated by the water-involved thermometer that is based on the Fe-Mg exchange between olivine and melt (Liu et al., 2017; Putirka et al., 2008; Sobolev et al., 2016).

The olivine liquidus temperature ($T_P^{ol/L}$) was first calibrated to the olivine crystallization temperature at 1 atm ($T_1^{ol/L}$) by the following equation:

$$T_1^{(ol/L)} = T_P^{(ol/L)} - 54P + 2P^2 \tag{3}$$

Mantle potential temperatures (T_p) were calculated from olivine liquidus temperatures at 1 atm ($T_1^{ol/L}$) using the following equation (Herzberg & Asimow, 2015):

$$T_P = 1.049 T_1^{ol/L} - 0.00019 (T_1^{ol/L})^2 + 1.487 * 10^{-7} (T_1^{ol/L})^3, \tag{4}$$

where P is the crystallization pressure of olivine in GPa, equaling roughly the crystallization pressure of cpx, which can be estimated from the equilibrium between the cpx and corrected melt compositions. All temperatures are in °C. Although the equation for the calculation of mantle potential temperatures was calibrated from experiments based on peridotite, the test of this equation on the pyroxenite-based experiments shows that it can give mantle potential temperatures within an uncertainty of ± 70 °C (Liu et al., 2017).

3. Results

3.1. Chemical Characteristics of High-Ti Picrites in the Emeishan LIP

The studied picrite samples are massive rocks with a porphyritic texture, containing abundant olivine, clinopyroxene, and spinel phenocrysts (Figure S2). Their bulk MgO contents range from 19.7 to 22.5 wt.% (Data Set S1), which are similar to the compositions obtained by previous investigations for bulk rocks and melt inclusions in olivine or spinel grains (Data Sets S1 and S2). Picrites have high Mg# (Mg# = Mg/(Mg + Fe)) of 69.5–82.5 and are generally in equilibrium with olivine with the highest Fo content in each sample (Figure S3a in Supporting Information S1). Fo values of Lijiang picrites are slightly lower than the equilibrium values, which indicates that the samples experienced a small degree of olivine accumulation. Similarly, the clinopyroxene phenocrysts in Dali and Binchuan picrites are almost close to equilibrium with the bulk-rock compositions (Figure S3b in Supporting Information S1), arguing against significant accumulation or fractionation of mafic minerals. For the Lijiang and Yongsheng samples, Mg# values of the cpx phenocrysts are lower than the equilibrium values, which could have been caused by early crystallization or accumulation of olivine.

High-Ti/Y picrites are characterized by Ti/Y ratios ranging from 526 to 727 (>500; Kamenetsky et al., 2012; Figure 1). The rocks show typical OIB-like trace element patterns in primitive mantle-normalized trace element diagrams (Figure 1) and their Nb/U and Ce/Pb ratios (Nb/U = 30–56, Ce/Pb = 16–21; Data Set S1) are comparable to the range of MORB and OIB (Hofmann et al., 1986), indicating insignificant crustal contamination.

3.2. Water in Clinopyroxene From High-Ti Picrites

As shown in Figure 2, the cpx phenocrysts in Lijiang and Yongsheng picrites show three groups of OH bands ($\sim 3,620$–$3,651$, $\sim 3,540$, and $\sim 3,460$ cm^{-1}), which are related to the Al^{3+} substitution in the Si tetrahedral site, metal (e.g., Ca) vacancies with tetrahedral Al^{3+}, and singly protonated Ca vacancies with a nearby octahedral M^{3+},
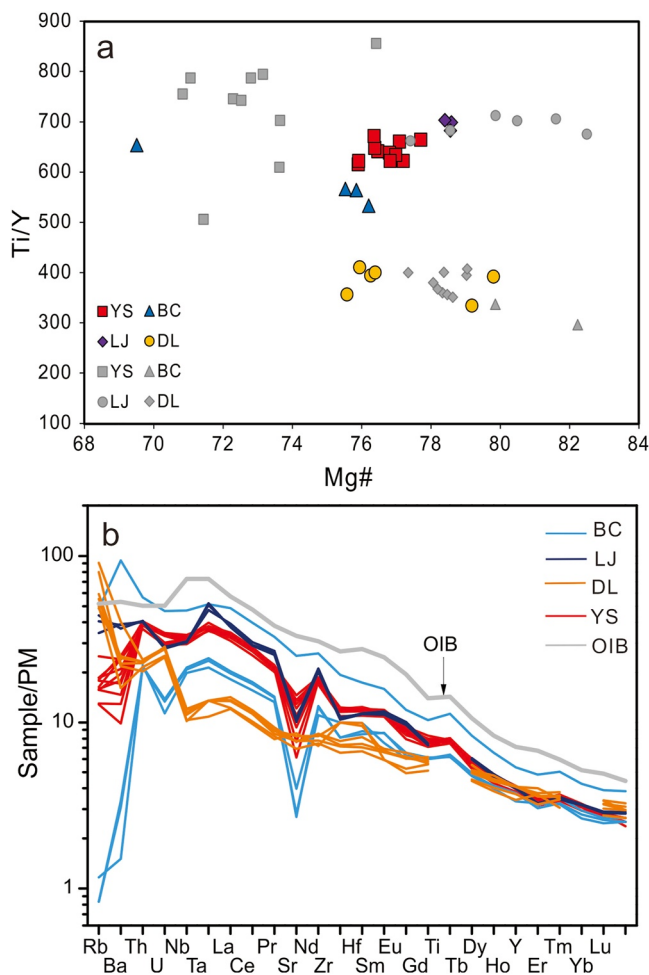
Figure 1. Major and trace element compositions of picrites from ELIP. (a) Ti/Y versus bulk-rock Mg# plot. (b) Primitive mantle-normalized trace element patterns. The symbols with color are samples studied in this work. Data sources: Dali (DL) from Liu et al. (2017); BC (Binchuan) from Yu et al. (2019); Lijiang (LJ) from Hanski et al. (2010); Yongsheng (YS) from this work. Gray symbols represent data from Hanski et al. (2010) and Kamenetsky et al. (2012). Normalization values for primitive mantle and OIB taken from McDonough and Sun (1995) and Sun and McDonough (1989), respectively.

respectively (e.g., Balan et al., 2020; Skogby et al., 1990; Yang et al., 2019). These spectra are comparable to those of cpx in Dali low-Ti picrites, Cenozoic basalts in eastern China and mantle xenoliths (Liu et al., 2015, 2017; Xia et al., 2013). Water contents of the cpx phenocrysts from Lijiang and Yongsheng high-Ti/Y picrites were calculated based on the Beer-Lambert law, unpolarized integral absorption area and absorption coefficient of Bell et al. (1995). The calculated water contents of these cpx phenocrysts range from 110 to 410 ppm (Figure 3) and are listed in Data Set S2.
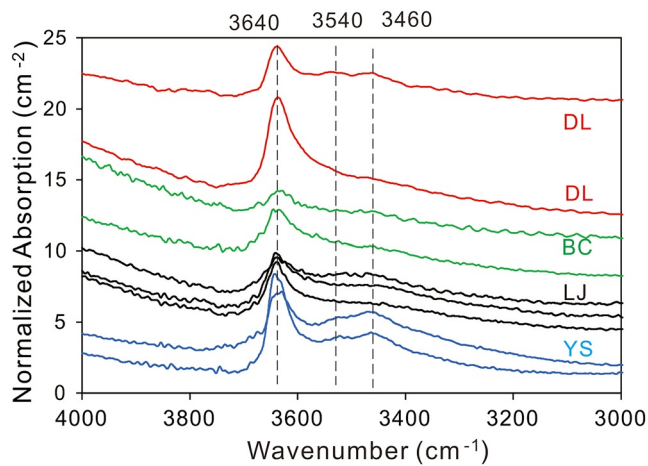
4. Discussion

4.1. Estimation of Magmatic Water Content From Clinopyroxene Phenocrysts

While the reverse calculation from clinopyroxene phenocryst compositions provides the only potential alternative approach to melt inclusion analysis for recovering the pre-erupted water content of basaltic melts (O'Leary et al., 2010; Wade et al., 2008), the major challenge of this method is the loss of water from clinopyroxene phenocrysts upon cooling of the lava (e.g., Liu et al., 2015; Lloyd et al., 2016; Turner et al., 2017). In the following, we show evidence that at least some clinopyroxene phenocrysts have preserved their initial water contents and hence can be used to obtain magmatic water contents for ELIP picrites.

In their calibration of the water partition coefficient between cpx and basaltic melt ($D^{cpx/melt}$), O'Leary et al. (2010) considered the hydroxyl defects related to both metal vacancies and the coupled Al substitution in the tetrahedral Si site. The preservation of correlation between water in cpx and $D^{cpx/melt}$ could be thus considered diagnostic evidence for that the cpx phenocrysts have preserved their original magmatic water content. This correlation could be identified for the cpx phenocrysts in a low-Ti/Y picrite sample from Dali (Figure 3), which indicates that water loss through diffusion was not significant in this case (Liu et al., 2017). However, for Binchuan, Lijiang, and Yongsheng picrites, the situation is a bit more complex. As shown in Figure 3, while many cpx phenocrysts from Binchuan picrites show relatively low water contents (<200 ppm), the cpx grains with the highest water content in each sample plot on the same line with an equilibrium magma water content of ~3.0 wt.%. In addition, these water contents are negatively correlated with cpx Mg#, which is consistent with a trend formed by crystal fractionation in a closed system (Wade et al., 2008). These two observations suggest that water diffusion in these cpx crystals was not significant. Thus, we use the

cpx crystals with the highest Mg# to calculate magma water contents for Binchuan picrites (Figure 3). Although this selection is slightly different from that employed by Yu et al. (2019), the resulting water content estimates are comparable (see Figure 3). Due to the heavy alteration and relative scarcity of cpx phenocrysts in Lijiang and Yongsheng picrites, we could not obtain as much data for them as for Dali and Binchuan picrites. In the Lijiang and Yongsheng samples, no correlation between H_2O and $D^{cpx/melt}$ and Mg# could be recognized. A profile analysis across a large cpx phenocryst (15EJH08B-1 with a dimension of ~1,000 μm) revealed that the water contents of the core and rim vary from 197 ± 40 to 140 ± 28 ppm (Data Set S2). This indicates that diffusion did occur to some extent. In such cases, we use the cpx grains with the highest water content to estimate the lower limit of the magmatic water content for the picrites from these two locations. Calculated water contents of the magma in equilibrium with the selected cpx phenocrysts and values corrected for the effects of olivine crystallization at an early stage are listed in Table 1.

As shown in Figure 4, the water contents of the primary magmas of high-Ti/Y picrites, which are in equilibrium with the mantle, are from 2.17 to 2.52 wt.%, which are considerably higher than the estimated water contents in MORB and OIB and reach the level of back-arc and/or island arc basalts. The lower-limit H_2O content is clearly

Figure 2. Typical OH bands of cpx phenocrysts in ELIP picrites. The spectra have been normalized to a thickness of 1 cm. The numbers mark the positions of typical OH bands in clinopyroxene crystals. The abbreviations represent the same sample locations as in Figure 1.

higher than the previously assumed H_2O level of ~0.3 wt.%, which was used in calculating T_p for picritic melts from the ELIP (Tao et al., 2015).

4.2. Wet Plume Source of High-Ti ELIP Picrites

The water concentrations of the primary magmas were used to recover the water contents of the respective mantle sources, based on the batch and fractional partial melting models (Shaw, 1970). The partition coefficient of H_2O between mantle rocks (pyroxenite or peridotite) and basaltic melt ranges from 0.0085 to 0.0129 (Hirschmann et al., 2009). One parameter that affects significantly the calculated water content in the mantle source is the estimated degree of partial melting (F). Petrological forward and inverse modeling based on major element compositions of magmas (e.g., PRIMELT3; Herzberg & Asimow, 2015) is frequently used to recover primary magma compositions in equilibrium with mantle rocks, calculate mantle T_p and degrees of partial melting. However, when this model (PRIMELTS MEGA.XLSM) was applied to the ELIP picrites of this study, "pyroxenite source" or "augite fractionation" warnings always appeared. Based on the recovered primary melt compositions and a previous version of the same model (PRIMELT2), the degree of partial melting for low-Ti type picrites at the bottom of the Binchuan volcanic sequence was estimated to be around 17% (Li et al., 2012).
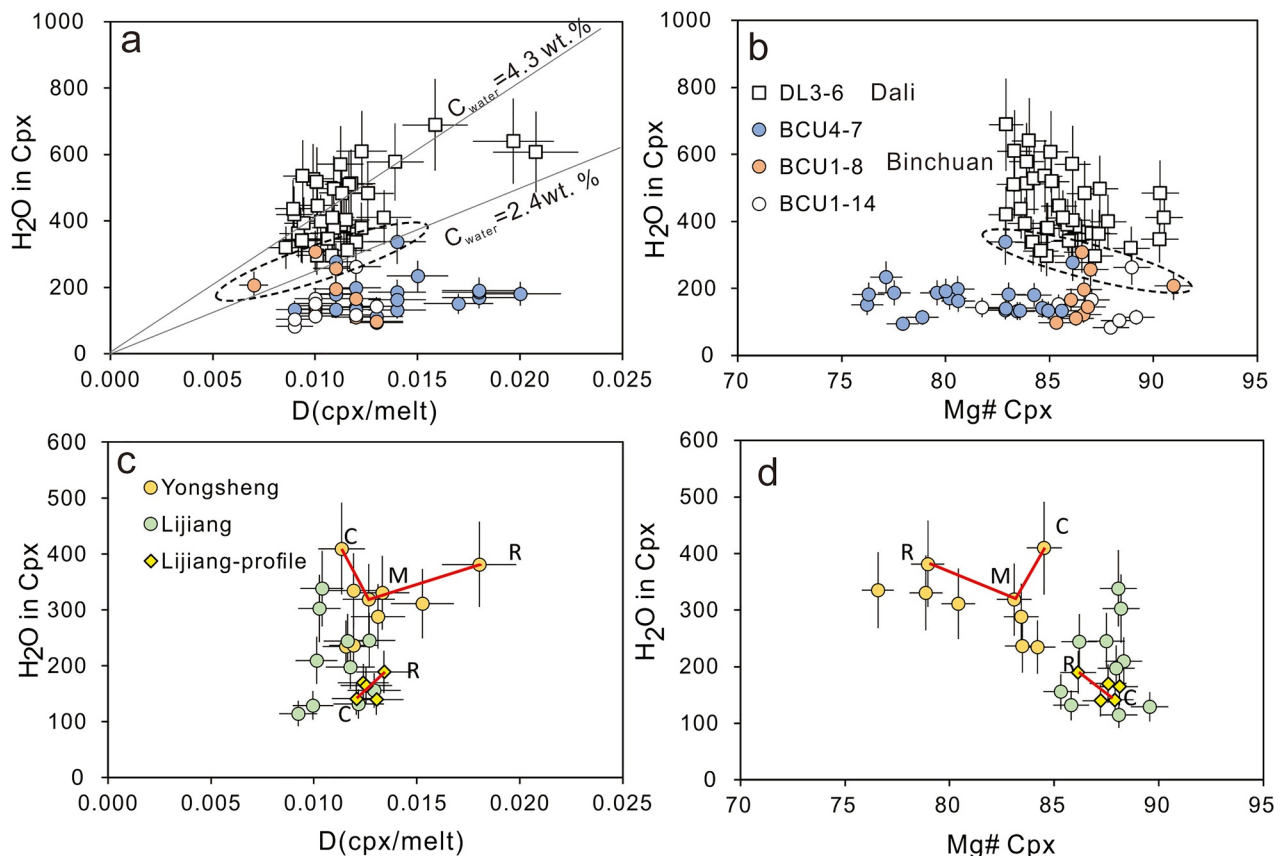
Figure 3. Comparison of water contents in clinopyroxene grains and the calculated partition coefficients of water between cpx and basaltic melt and cpx Mg#. (a, b) Picrites from Dali and Binchuan. The data for DL3-6 are from Liu et al. (2017) and for Binchuan picrites from Yu et al. (2019). The $D^{(cpx/melt)}$ is calculated by Equation 10 in O'Leary et al. (2010). The cpx grains within the dotted ellipses in a and b are the same cpx grains. (c, d) Picrites from Lijiang and Yongsheng. The red lines connect analytical spots from the same cpx crystals. C, M, and R represent core, mantle, and rim, respectively. The LJ profile represents multiple analyses from a single cpx grain in a Lijiang picrite sample (15-EJH-08B-1). The uncertainty (2SD) of the vertical axis, $D^{(cpx/melt)}$ and Mg# is ±20%, ±10%, and ±1%, respectively.

Table 1
*Summary of Compositional Data of Picrites From the ELIP and Calculated Water Contents in the Mantle Source*

Location	Ti/Y	2SD	Sm/Yb	2SD	TiO_2/Al_2O_3	2SD	Highest Mg# of cpx	Highest Fo of olivine
Dali	400	25	1.88	0.09	0.23	0.02	91.1	93.4
Binchuan	622	40	3.5	0.18	0.18	0.02	91.0	91.1
Yongsheng	714	17	3.77	0.19	0.21	0.02	84.5	91.9
Lijiang	737	8	3.67	0.18	0.11	0.01	89.6	91.1

Location	Water content	Ol fractionation	Ol corrected	H_2O/Ce	Partial melting degree		Water in mantle source	
					$F1$	$F2$	$C_{water\ in\ source}$ $(F1)$	$C_{water\ in\ source}$ $(F2)$
Dali	3.73	0.10	3.36	1,811	0.18	0.18	6,446	6,446
Binchuan	2.71	0.07	2.52	969	0.22	0.14	5,721	3,723
Yongsheng	3.60	0.37	2.27	493	0.22	0.14	5,153	3,354
Lijiang	3.10	0.30	2.17	452	0.22	0.14	4,926	3,206

Note. The amount of olivine fractionation is calculated using PRIMELT3 (Herzberg & Asimow, 2015). The water content of the mantle source is calculated based on the batch partial melting model. Water partitioning coefficients are discussed in the main text.

The PRIMELT3 model conducted for a Binchuan sample (DY8-7) resulted in an *F* value of ~18%, without an error warning. As shown in Table 1, except for TiO_2 and trace elements, the high-Ti/Y picrites of this study show similar concentrations of SiO_2, FeO, MgO, CaO, and Al_2O_3 to those of low-Ti/Y picrite (DY8-7 by Li et al., 2012; Data Set S1), and therefore the degree of partial melting for high-Ti/Y picrite is probably also around 18%. This
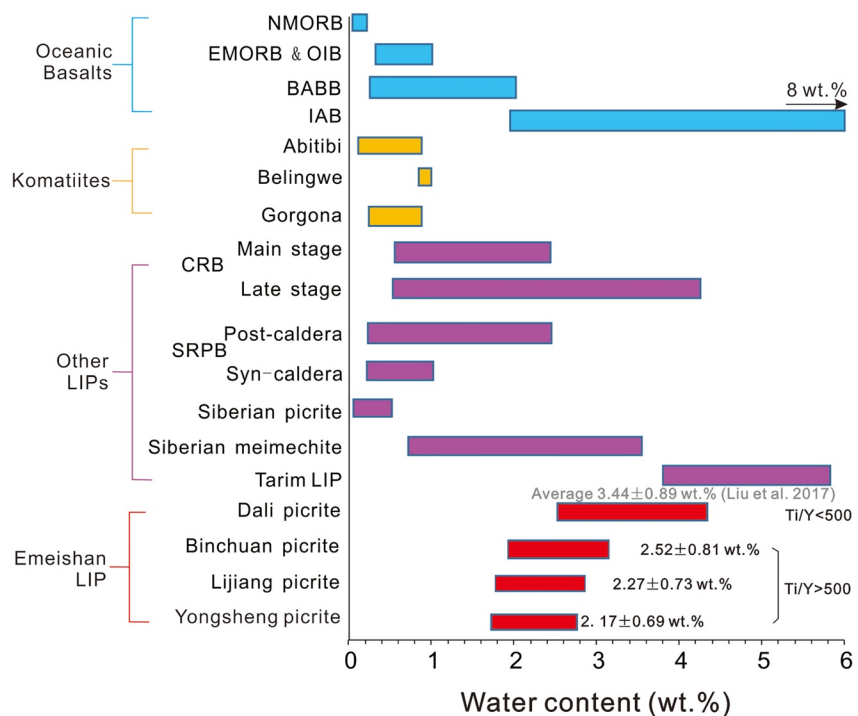
Figure 4. Comparison of H_2O contents in primitive magmas from the ELIP and other geological settings. The Yongsheng and Lijiang data are from this work and the Dali data from Liu et al. (2017). The original Binchuan data are from Yu et al. (2019) and recalculated data from this work. The water abundance data for oceanic basalts are from Dixon et al. (2004), for komatiites from Kamenetsky et al. (2010), Shimizu et al. (2001), and Sobolev et al. (2016) and for other LIPs from the compilation of Liu et al. (2017). Abbreviations: NMORB, normal mid-ocean ridge basalt; EMORB, enriched mid-ocean ridge basalt; OIB, oceanic island basalt; BABB, back-arc basin basalt; CRB, Columbia River basalt; SRPB, Snake River Plain basalt. For the compiled data, see Data Set S3.
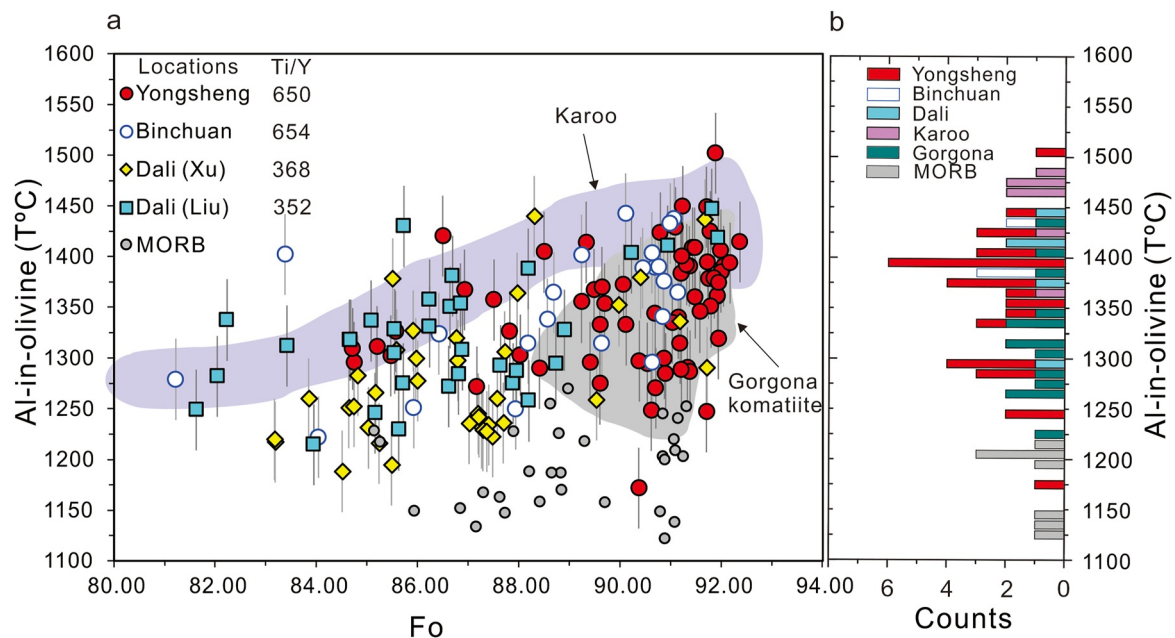
Figure 5. Crystallization temperatures of olivine phenocrysts in picrites from the ELIP based on the Al partitioning between olivine and coexisting spinel. (a) Calculated temperature versus Fo content of olivine. Crystallization temperatures of Karoo picrites, Gorgona komatiites, and MORB are shown for comparison, with data taken from Heinonen et al. (2015) and Coogan et al. (2014). The Dali (Xu) data are from Xu and Liu (2016), the Dali (Liu) data from Liu et al. (2017), and the Yongsheng and Binchuan data from this study. All data are presented in Data Set S2. (b) Histogram for crystallization temperatures of olivine phenocrysts with Fo > 90 mol.%.

simplification inescapably induces some additional uncertainty. To estimate the minimum water content in the mantle source, we consider the degree of partial melting for the high-Ti/Y picrite sample to be in the range of 14–22%. As shown in Table 1, the lowest water contents of the mantle sources for the Binchuan, Yongsheng, and Lijiang picrites are estimated to be 3,196 ± 1,278, 2,635 ± 1,054, and 1,802 ± 721 ppm, respectively (Table 1). These values are considerably higher than the water contents of the global MORB and OIB sources (Hirschmann, 2006), indicating that high-Ti/Y picrites were derived from mantle sources that were extensively hydrated, although they are lower than the value obtained for the source of the low-Ti picrites from Dali (at the bottom of the Binchuan volcanic section; >6,000 ppm; Liu et al., 2017).

The water enrichment in the mantle source of the studied high-Ti/Y picrites could be a result of several different processes including, for instance, metasomatism of the lithospheric mantle by fluids/hydrous melts in a subduction setting (Cox et al., 1967; Grove & Parman, 2004) or entrapment of hydrous mantle transition zone (MTZ) segments/melt by an ascending mantle plume (Liu et al., 2017; Sobolev et al., 2016). The Nb/U (30–56) and Ce/Pb (16–21) ratios of all high-Ti/Y picrites are rather close to the values of MORB and OIB (40 ± 7 for Nb/U, 25 ± 5 for Ce/Pb; Hofmann et al., 1986), which are considerably higher than the values of typical arc or back-arc basalts (~<5; Tatsumi, 2005). This observation argues strongly against the role of the metasomatized continental lithospheric mantle as the main source of water.

In the following discussion, we present additional observations on the mantle temperature and the origin of recycled material in support of the hydrous mantle plume model. First, we have calculated olivine crystallization temperatures for the studied picrites using the Al-in-olivine thermometer (Coogan et al., 2014) and high-precision Al_2O_3 contents in olivine, which allow the estimation of the olivine crystallization temperature with an uncertainty better than ±40 °C. The spinels analyzed in this study exhibit stoichiometrically calculated Fe^{3+}/Fe_T values in the range of 0.22–0.42, and some of them exceed the Fe^{3+}/Fe_T calibration range of the thermometer (<0.35; Coogan et al., 2014). However, we note that many spinel analyses from the LIPs data sets of Coogan et al. (2014) (Gorgana komatiites, Madagascar, Baffin Island, and Greenland) show Fe^{3+}/Fe_T higher than 0.35 (up to 0.46), while they give consistently higher estimates of olivine crystallization temperature than MORB (Figure 5; Coogan et al., 2014). Thus, we suggest a small excess in Fe^{3+}/Fe_T would not lead to systematical errors in our temperature calculation. On the other hand, the Cr# values (Cr# = Cr/(Cr + Al), in atom number)

of our samples are in the range of 0.63–0.82, and the dominant values are lower than 0.78 (Data Set S2), which is similar to the case of Karoo picrites (0.64–0.78, Heinonen et al., 2015). Heinonen et al. (2015) showed that the spinel grains with high Cr# give meaningful estimation of olivine crystallization temperature, based on the linear correlation of Cr# and partitioning of Al between olivine and spinels (Wan et al., 2008) and the observations that the calculated temperatures do not correlate with Cr#. For our samples, similarly, there is no clear dependence of calculated temperatures on Cr# (Figure S4). As shown in Figure 5, the calculated crystallization temperatures for olivine phenocrysts from different ELIP picrites generally increase with increasing of Fo, which are consistent with the expected cooling during magma evolution. These calculated temperatures also converge at $1,450 \pm 40$ °C, which is comparable with that of Karoo and Gorgona komatiites. This temperature exceeds that of MORB by 200 °C (Coogan et al., 2014) and is consistent with the maximum temperature (1,440 °C) calculated by Xu and Liu (2016) for Emeishan picrites using the same method. These observations allow us to conclude that our estimates of olivine crystallization temperatures are valid.

We applied the relationship between the mantle T_p and olivine liquidus temperature to estimate the corresponding mantle T_p for the ELIP, yielding $1,501 \pm 70$ °C (see the Section 2). This T_p estimate is consistent, within the uncertainty, with that obtained for the Dali low-Ti/Y picrites ($1,500 \pm 70$ °C) by the same method (Liu et al., 2017). In this study, the olivine phenocrysts with high Fo (>91) show significantly higher NiO (0.38–0.49 wt.%) and Fe/Mn (66.5–81.0; Data Set S2) compared to olivine in MORB (NiO 0.24–0.38 wt.%, Fe/Mn 62.4 ± 2.5; Sobolev et al., 2007), indicating some contribution from a pyroxenite component in a peridotite source. Although the variation of NiO and MnO in olivine could be partly explained by different conditions (P, T, fO_2) of partial melting, as discussed in detail by Liu et al. (2017), the systematically higher NiO and Fe/Mn in olivine grains from the high-Ti/Y picrites compared to olivine grains from both Archean and Phanenozoic komatiites show that these parameters at least reflect source heterogeneity or they can be considered indications of the maximum proportions of pyroxenite-derived melt (Liu et al., 2017). The mantle source enrichment by recycled oceanic eclogite/pyroxenite is also supported by the observation that olivine phenocrysts in many ELIP picrites with positive Nb and Ta anomalies show $\delta^{18}O$ values higher than those of the normal mantle (Yu et al., 2017), which are principally associated with the interaction of rocks with the Earth's hydrosphere (Taylor & Simon, 1986). In summary, we suggest that the studied high-Ti/Y picrites were derived from a hydrous, eclogite/pyroxenite-bearing mantle plume, which was in this respect similar to the source of the low-Ti/Y picrites in the Dali area (Liu et al., 2017).

4.3. Geochemical Variations Coupled With Water in the Mantle Source

For an eclogite/pyroxenite-bearing and dry mantle plume, the geochemical characteristics of the final partial melts would be physically controlled by the difference between the solidus temperatures of different lithologies along an adiabatic decompressional thermal gradient (Lambart et al., 2016; Sobolev et al., 2007). It has been concluded that the mantle sources of Archean and Phanerozoic komatiites were extensively hydrated but had a major element composition close to that of peridotite (Gurenko et al., 2016; Shimizu et al., 2001; Sobolev et al., 2016). Recent work indicates that a similarly hydrous source played an important role in the genesis of many Phanerozoic LIPs (Liu et al., 2017). Water in an eclogite/pyroxenite-bearing mantle plume would be an additional factor modifying the proportions of partial melts derived from different lithologies along the melting column, due to its large effects on the solidus temperature (Asimov & Langmuir, 2003; Hirose, 1997; Hirschmann, 2006; Katz et al., 2003). Consequently, it can be expected that the major or trace element composition of a primary magma would be closely related to the water content of its mantle source.

As shown in Figure 6, the estimated water content in the mantle source decreases and the bulk-rock Ti/Y, Sm/Yb, and TiO_2/Al_2O_3 ratios increase from the Dali low-Ti picrites in the bottom part of the Binchuan volcanic section to the Binchuan high-Ti picrites in the upper part of the same section. In the following, we first discuss the currently existing models for the variations in elemental ratios. The observed variation in the elemental ratios for the Binchuan eruption sequence could be explained by that the high-Ti picrites were laterally flowed from the periphery of the mantle plume head, where the lithosphere is thinner (Buchan & Ernst, 2019). However, this model cannot be reconciled with the observation that picrites in the ELIP only occur in its central zone (Hanski et al., 2010), with a larger extent of crustal elevation relative to other regions before the initiation of the ELIP took place (He et al., 2003). Due to the fact that Ti (Sm) is less compatible than Y (Yb) during partial melting of both peridotite or pyroxenite (Salters & Stracke, 2004), the temporal and spatial variations in chemical composition would also be explained by different extents of partial melting. Progressive lithospheric thinning and the
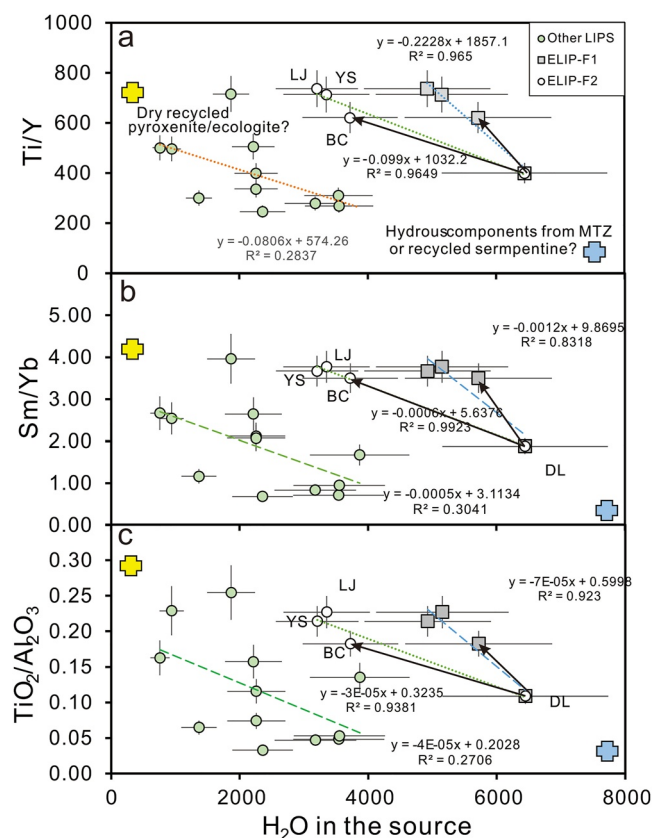
Figure 6. Comparison of water contents (ppm) in mantle sources and selected trace-element and major-element ratios for LIPs and OIBs. (a) Water contents of mantle sources compared with bulk-rock Ti/Y. ELIP-F1 and ELIP-F2 mean two sets of calculation of the water content in the mantle sources, in which the degree of partial melting (F) is set at the values listed in Table 1. The uncertainty of the water contents for ELIP picrites, which were based on the clinopyroxene-method, is assumed to be 35% (2SD) and for the others, 20% (2SD). The error bars for the trace element ratio are less than 10% (2SD). The dashed lines show linear regressions. The bold arrows show timing from early eruptions (located in the lower part of the volcanic section) to late eruptions (located in the upper part of the volcanic section) in the specific LIPs. The blue bold cross indicates the hydrous component in the deep mantle, which would be associated with the mantle transition zone or recycled hydrated oceanic lithospheric mantle (Gurenko et al., 2016; Sobolev et al., 2016). The yellow bold cross represents fertile but dry pyroxenite in the mantle (Bizimis & Peslier, 2015). (b) Water contents of the mantle sources compared with bulk-rock Sm/Yb. (c) Water contents of the mantle sources compared with bulk-rock TiO_2/Al_2O_3. All the error bars are the same as in (a). Data sources: Cabato et al. (2015), Gurenko et al. (2016), Heinonen and Luttinen (2008), Leeman et al. (2009), (Sobolev et al., 2009, 2015, 2016, 2019), Stefano et al. (2011), and Trela et al. (2017). Trace elemental ratios are listed in Data Set S3 and Table 1.

consequent increase in the degree of partial melting at a shallower depth have been regarded as the main reasons for the observed temporal decline in Sm/Yb in many LIPs (Ernst, 2014; Lassiter & DePaolo, 1997; Ren et al., 2017). However, for the ELIP case, this explanation seems not to be in line with the following considerations. First, our modeling calculations show that for degrees of partial melting from 10% to 30%, the Ti/Y and Sm/Yb ratios would not be fractionated significantly during decompressional partial melting of an ascending mantle plume, for both peridotite or pyroxenite sources (Figures 7a and 7b). Second, the numerical modeling of the mantle plume head-lithosphere interaction shows that erosion caused by the impact of a plume head on a hydrated lithosphere is rather limited (Wang et al., 2015) within the time scale (<1 Ma) of the volcanism in the studied ELIP eruption sequence (Zhong et al., 2014).

It has been recognized for a long time that mantle plumes contain some amounts of recycled fertile components, such as eclogite/pyroxenite (Lin & van Keken, 2005; Sobolev et al., 2007), and it has been suggested that the thickness of the lithosphere is the main reason that moderates the proportion of pyroxenite-derived melts (Sobolev et al., 2007). In Data Set this scenario, the LIPs on a thicker lithosphere would have a higher fraction of melts from pyroxenite, leading to higher Ti/Y and Sm/Yb ratios. Model calculations by Melt-PX (Lambart et al., 2016) on partial melting of a two-lithology (pyroxenite and KLB1 fertile peridotite) mantle plume under dry conditions also support this view (Figure 7; see the Section 2 for modeling details). However, this predicted trend is contrary to the observation that picrites and basalts in the ELIP are transformed from the low-Ti/Y type to the high-Ti/Y type (Xu et al., 2001; Figure 6). This means that the variations in Ti/Y and Sm/Yb and their sharp shift within the eruption sequence could not be explained simply by adiabatic decompressional partial melting of a dry mantle plume, although the major element composition of the plume could be rather heterogeneous.

Thus, the variations in Ti/Y of lavas in the Emeishan LIP over the 1 Ma eruptional history could be best explained by compositional heterogeneities in the mantle sources. Based on the observed correlations between major and trace elemental ratios and the water contents in the mantle source (Figure 6), we suggest an alternative model. It explains these correlations and also the temporal variation in the geochemistry of the erupted lavas from a specific LIP as the result of variation in the mantle source components, including both the proportion of eclogite/pyroxenites and the water content of the mantle (Figure 8). In this model, the high water content and the low-Ti/Y endmember could be explained by hydrous peridotite, which is represented by the mantle sources of Archean or Cretaceous komatiites, containing thousands of ppm of water (Gurenko et al., 2016; Sobolev et al., 2016). On the other hand, the relatively low water content but the high-Ti/Y endmember could be attributed to recycled eclogite/pyroxenite, as indicated by several lines of petrological, geochemical, and seismic evidence to be present in upwelling mantle plumes (Lin & van Keken, 2005; Sobolev et al., 2007).

The water-rich components could potentially derive from the mantle transition zone (MTZ; Pearson et al., 2014; Sobolev et al., 2016) or the LLSVP in the lower mantle that was replenished by ultrahigh-pressure hydrous phases (phase H, phase δ, or H-δ solid solution) transported into the lower mantle by a subducted oceanic plate (Garnero et al., 2016; Herzberg, 2016). These two origins need not to be mutually exclusive. However, it has been shown that the MTZ is not pervasively hydrated (Yoshino et al., 2008), which is not consistent with widespread hydration of the mantle sources of LIPs. In addition, based on the assumption of an average upwelling velocity of 100 cm yr^{-1} and water diffusivity of
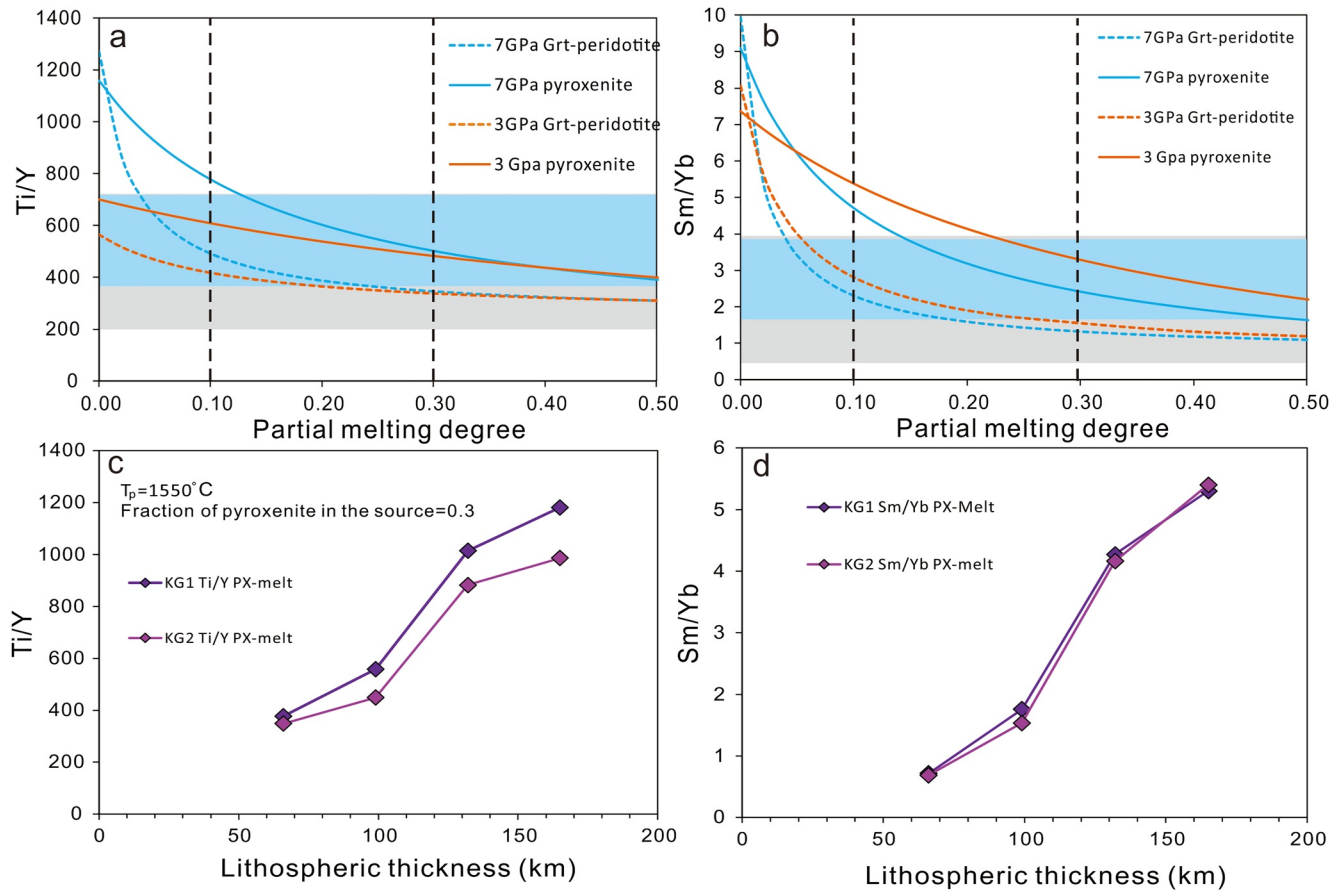
Figure 7. Modeled Ti/Y and Sm/Yb ratios for partial melts of peridotite and pyroxenite. (a, b) Covariation of modeled Ti/Y and Sm/Yb with the degree of partial melting. The blue and orange lines show how these two ratios change with partial melting of pure peridotite and pyroxenite at different pressures. The blue and gray regions indicate elemental ratios for the ELIP and global LIPs, respectively. The parameters and relevant data are presented in Data Set S4. (c, d) Variation of Ti/Y and Sm/Yb with the lithospheric thickness in regions where LIPs occur. The diamonds connected with lines show how the mixed accumulated melts derived from pyroxenite (KG1 and KG2) and fertile peridotite (KLB-1) vary during decompressional partial melting of a dry and lithologically heterogenous mantle plume. Each data point represents the value of a mixed melt if separated from the source at that depth. See Data Set S5 for more details.

10^{-8}–10^{-5} m^2 s^{-1}, Bercovici and Karato (2003) suggested that upon passing through the MTZ, a hot plume could not get a significant amount of water from the MTZ. Thus, we prefer that the water-rich components would come from a hydrous reservoir in the lower mantle, for instance the LLSVP, where most plume heads have originated. Based on direct observations of a seismic low-velocity layer directly above the MTZ and the prominent 520-km discontinuity, the existence of a volatile-rich and compositionally buoyant plume from the lower mantle beneath Ethiopia and East Africa has recently been suggested (Thompson et al., 2015). A similar low-velocity layer has also been found beneath some other Mesozoic flood basalt provinces, which have been explained by dehydration of water-bearing silicates in the responsible mantle plumes, although the spatial correlation requires the controversial assumption of long-term coupling of the continental lithosphere and the underlying mantle to depths of ~400 km (Vinnik & Farra, 2007). These seismic low-velocity layers atop the 410-km discontinuity beneath the LIPs would provide independent support for hydrous mantle plumes, which is consistent with the predicted partial melting depth for hydrous peridotite along a plume geothermal gradient (Katz et al., 2003).

5. Concluding Remarks

The high-Ti/Y picrites in the Emeishan large igneous province can have primary water contents of 2.1–2.5 wt.%. The corresponding water content of the mantle sources is higher than 3,000 ppm, which are considerably higher than that of the MORB source and the upper limit of the previously estimated water content of the OIB sources. The calculated water contents of the mantle sources are negatively correlated with Ti/Y, Sm/Yb, and TiO$_2$/Al$_2$O$_3$.
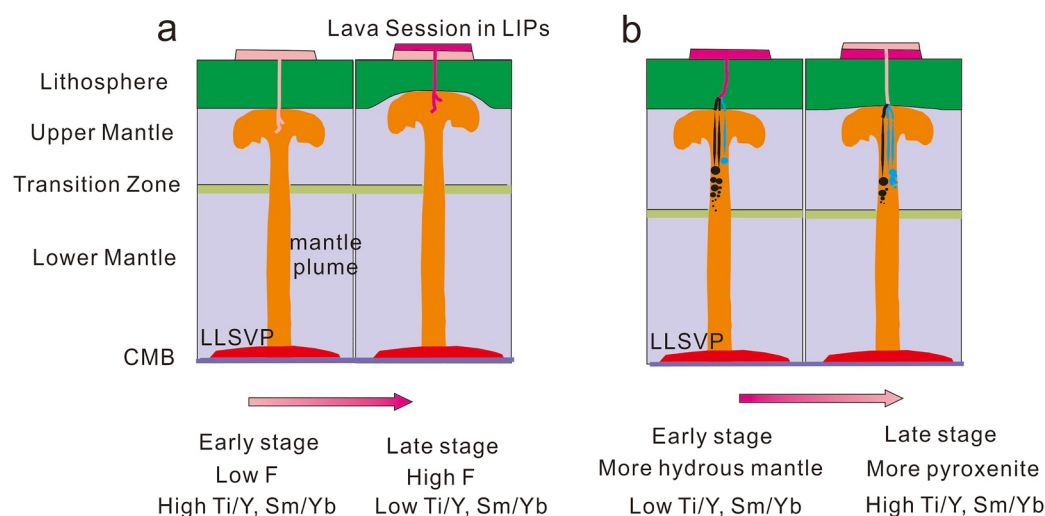
Figure 8. Schematic diagrams showing how a mantle plume can affect the compositional variation of picrite in the ELIP. CMB is the core-mantle boundary. To better demonstrate the details of the model, the dimensions of the mantle are not to scale. (a) Traditional explanation for the decrease in Ti/Y and Sm/Yb in ELIP picrite eruption sequences. In this model, an increasing degree of partial melting at a shallower depth for the melting column is suggested, which is usually attributed to the lithospheric thinning due to plume-lithosphere interaction. (b) New explanation for the temporal variation in Ti/Y and Sm/Yb in basalts/picrites in a rapidly erupted volcanic succession, resulting from partial melting of a hydrous, eclogite/pyroxenite-bearing mantle plume, as in the case of the Binchuan volcanic sequence in the Emeishan LIP. The dark dots and dark narrow vertical bands represent partial melting of the hydrous portion of the plume and subsequent melt accumulation and segregation from the source. The blue dots and blue vertical bands represent partial melts of pyroxenite and their segregation. More melts coming from hydrous mantle can contribute to lower Ti/Y and Sm/Yb ratios of the final mixed melts.

The large variation of these elemental ratios could not be simply explained by different degrees of partial melting of a single peridotite or pyroxenite source, or simply by a decrease in the proportion of pyroxenite-derived melts during the thinning of the lithosphere. Instead, the correlations between the water contents and chemical compositions could be best explained by partial melting of two end-member sources: one is hydrous peridotite and the other is relatively dry pyroxenite.

Whether this model could be applied to the global LIPs needs further detailed studies on the water content of primitive lava samples with a clear sequence information, as the present data from LIPs other than the ELIP (Figure 6) cannot not provide convincing answers yet. However, the ELIP case study shows that the compositional variations of primitive magmas within a specific LIP during a rather short time period can be related to the time dependence of plume material (hydrous peridotite versus pyroxenite) rising from deeper to shallower levels, rather than strong erosional interaction between the lithosphere and a mantle plume.

Conflict of Interest

The authors declare no conflicts of interest relevant to this study.

Data Availability Statement

The Supporting Data sets for this research are available via the DOI (https://doi.org/10.6084/m9.figshare.14815878).

References

Asimow, P. D., & Langmuir, C. H. (2003). The importance of water to oceanic mantle melting regimes. *Nature*, *7*, 815–820. https://doi.org/10.1038/nature01429

Balan, E., Paulatto, L., Liu, J., & Ingrin, J. (2020). Low-temperature infrared spectrum and atomic-scale structure of hydrous defects in diopside. *European Journal of Mineralogy*, *32*(5), 505–520. https://doi.org/10.5194/ejm-32-505-2020

Bell, D. R., Ihinger, P. D., & Rossman, G. R. (1995). Quantitative analysis of trace OH in garnet and pyroxenes. *American Mineralogist*, *80*(5–6), 465–474.

Bercovici, D., & Karato, S. I. (2003). Whole-mantle convection and the transition-zone water filter. *Nature*, *425*(6953), 39–44. https://doi.org/10.1038/nature01918

Bizimis, M., & Peslier, A. H. (2015). Water in Hawaiian garnet pyroxenites: Implications for water heterogeneity in the mantle. *Chemical Geology*, *397*, 61–75. https://doi.org/10.1016/j.chemgeo.2015.01.008

Bryan, S., & Ernst, R. E. (2008). Revised definition of large igneous provinces (LIPs). *Earth-Science Reviews*, *86*, 175–202. https://doi.org/10.1016/j.earscirev.2007.08.008

Buchan, K. L., & Ernst, R. E. (2019). Giant circumferential dyke swarms: Catalogue and characteristics. In R. K. Srivastava, R. E. Ernst, & P. Peng (Eds.), *Dyke swarms of the world: A modern perspective* (pp. 14–44). Springer https://doi.org/10.1007/978-981-13-1666-1_1

Burke, K., Steinberger, B., Torsvik, T. H., & Smethurst, M. (2008). Plume generation zones at the margins of large low shear velocity provinces on the core–mantle boundary. *Earth and Planetary Science Letters*, *265*, 49–60. https://doi.org/10.1016/j.epsl.2007.09.042

Cabato, J. A., Stefano, C. J., & Mukasa, S. B. (2015). Volatile concentrations in olivine-hosted melt inclusions from the Columbia River flood basalts and associated lavas of the Oregon Plateau: Implications for magma genesis. *Chemical Geology*, *392*, 59–73. https://doi.org/10.1016/j.chemgeo.2014.11.015

Coogan, L. A., Saunders, A. D., & Wilson, R. N. (2014). Aluminum-in-olivine thermometry of primitive basalts: Evidence of an anomalously hot mantle source for large igneous provinces. *Chemical Geology*, *368*, 1–10. https://doi.org/10.1016/j.chemgeo.2014.01.004

Cox, K. G., MacDonald, R., & Hornung, G. (1967). Geochemical and petrological provinces in the Karoo basalts of southern Africa. *American Mineralogist*, *52*, 1451–1474.

Dixon, J. E., Dixon, T. H., Bell, D. R., & Malservisi, R. (2004). Lateral variation in upper mantle viscosity: Role of water. *Earth and Planetary Science Letters*, *222*, 451–467. https://doi.org/10.1016/j.epsl.2004.03.022

Ernst, R. E. (2014). *Large igneous provinces*. Cambridge University Press.

Garnero, E. J., McNamara, A. K., & Shim, S. H. (2016). Continent-sized anomalous zones with low seismic velocity at the base of Earth's mantle. *Nature Geoscience*, *9*(7), 481–489. https://doi.org/10.1038/ngeo2733

Grove, T. L., & Parman, S. W. (2004). Thermal evolution of the Earth as recorded by komatiites. *Earth and Planetary Science Letters*, *219*, 173–187. https://doi.org/10.1016/s0012-821x(04)00002-0

Gurenko, A. A., Kamenetsky, V. S., & Kerr, A. C. (2016). Oxygen isotopes and volatile contents of the Gorgona komatiites, Colombia: A confirmation of the deep mantle origin of H_2O. *Earth and Planetary Science Letters*, *454*, 154–165. https://doi.org/10.1016/j.epsl.2016.08.035

Hanski, E., Kamenetsky, V. S., Luo, Z. Y., Xu, Y. G., & Kuzmin, D. V. (2010). Primitive magmas in the Emeishan large igneous province, southwestern China and northern Vietnam. *Lithos*, *119*, 75–90. https://doi.org/10.1016/j.lithos.2010.04.008

Hawkesworth, C. J., Lightfoot, P. C., Fedorenko, V. A., Blake, S., Naldrett, A. J., Doherty, W., & Gorbachev, N. S. (1995). Magma differentiation and mineralization in the Siberian continental basalts. *Lithos*, *34*, 61–88. https://doi.org/10.1016/0024-4937(95)90011-x

He, B., Xu, Y. G., Chung, S. L., Xiao, L., & Wang, Y. (2003). Sedimentary evidence for a rapid, kilometer-scale crustal doming prior to the eruption of the Emeishan flood basalts. *Earth and Planetary Science Letters*, *213*, 391–405. https://doi.org/10.1016/s0012-821x(03)00323-6

Heinonen, J. S., Jennings, E. S., & Riley, T. R. (2015). Crystallisation temperatures of the most Mg-rich magmas of the Karoo LIP on the basis of Al-in-olivine thermometry. *Chemical Geology*, *411*, 26–35. https://doi.org/10.1016/j.chemgeo.2015.06.015

Heinonen, J. S., & Luttinen, A. V. (2008). Jurassic dikes of Vestfjella, Western Dronning Maud Land, Antarctica: Geochemical tracing of ferropicrite sources. *Lithos*, *105*(3–4), 347–364. https://doi.org/10.1016/j.lithos.2008.05.010

Herzberg, C. (2016). Petrological evidence from komatiites for an early Earth carbon and water cycle. *Journal of Petrology*, *57*(11), 2271–2288. https://doi.org/10.1093/petrology/egw055

Herzberg, C., & Asimow, P. D. (2015). PRIMELT 3 MEGA.XLSM software for primary magma calculation: Peridotite primary magma MgO contents from the liquidus to the solidus. *Geochemistry, Geophysics, Geosystems*, *16*, 563–578. https://doi.org/10.1002/2014GC005631

Hirose, K. (1997). Melting experiments on lherzolite KLB-1 under hydrous conditions and generation of high-magnesian andesitic melts. *Geology*, *25*, 42–44. https://doi.org/10.1130/0091-7613(1997)025<0042:meolku>2.3.co;2

Hirschmann, M. M. (2006). Water, melting, and the deep Earth H_2O cycle. *Annual Review of Earth and Planetary Sciences*, *34*, 629–653. https://doi.org/10.1146/annurev.earth.34.031405.125211

Hirschmann, M. M., Tenner, T., Aubaud, C., & Withers, A. C. (2009). Dehydration melting of nominally anhydrous mantle: The primacy of partitioning. *Physics of the Earth and Planetary Interiors*, *176*, 54–68. https://doi.org/10.1016/j.pepi.2009.04.001

Hofmann, A. W., Jochum, K. P., Seufert, M., & White, W. M. (1986). Nb and Pb in oceanic basalts: New constraints on mantle evolution. *Earth and Planetary Science Letters*, *79*, 33–45. https://doi.org/10.1016/0012-821x(86)90038-5

Ingrin, J., Latrous, K., Doukhan, J. C., & Doukhan, N. (1989). Water in diopside: An electron microscopy an infrared spectroscopy study. *European Journal of Mineralogy*, *1*, 327–342. https://doi.org/10.1127/ejm/1/3/0327

Ivanov, A. V., Mukasa, S. B., Kamenetsky, V. S., Ackerson, M., Demonterova, E. I., Pokrovsky, B. G., et al. (2018). Volatile concentrations in olivine-hosted melt inclusions from meimechite and melanephelinite lavas of the Siberian Traps Large Igneous Province: Evidence for flux-related high-Ti, high-Mg magmatism. *Chemical Geology*, *483*, 442–462. https://doi.org/10.1016/j.chemgeo.2018.03.011

Jourdan, F., Bertrand, H., Schärer, U., Blichert-Toft, J., Féraud, G., & Kampunzu, A. B. (2007). Major and trace element and Sr, Nd, Hf, and Pb isotope compositions of the Karoo large igneous province, Botswana–Zimbabwe: Lithosphere vs mantle plume contribution. *Journal of Petrology*, *48*, 1043–1077. https://doi.org/10.1093/petrology/egm010

Kamenetsky, V. S., Chung, S. L., Kamenetsky, M. B., & Kuzmin, D. (2012). Picrites from the Emeishan large igneous province, SW China: A compositional continuum in primitive magmas and their respective mantle sources. *Journal of Petrology*, *53*, 2095–2113. https://doi.org/10.1093/petrology/egs045

Kamenetsky, V. S., Gurenko, A. A., & Kerr, A. C. (2010). Composition and temperature of komatiite melts from Gorgona Island, Colombia, constrained from olivine-hosted melt inclusions. *Geology*, *38*, 1003–1006. https://doi.org/10.1130/G31143.1

Katz, R. F., Spiegelman, M., & Langmuir, C. H. (2003). A new parameterization of hydrous mantle melting. *Geochemistry, Geophysics, Geosystems*, *4*, 1073. https://doi.org/10.1029/2002GC000433

Keppler, H., & Rauch, M. (2000). Water solubility in nominally anhydrous minerals measured by FTIR and 1H MAS NMR: The effect of sample preparation. *Physics and Chemistry of Minerals*, *27*, 371–376. https://doi.org/10.1007/s002699900070

Lambart, S., Baker, M. B., & Stolper, E. M. (2016). The role of pyroxenite in basalt genesis: Melt-PX, a melting parameterization for mantle pyroxenites between 0.9 and 5 GPa. *Journal of Geophysical Research: Solid Earth*, *121*, 5708–5735. https://doi.org/10.1002/2015JB012762

Lassiter, J. C., & DePaolo, D. J. (1997). Plume/lithosphere interaction in the generation of continental and oceanic flood basalts: Chemical and isotopic constraints. In J. Mahoney, & F. Coffin (Eds.), *Large igneous provinces: Continental, oceanic, and planetary flood volcanism* (Vol. 100, pp. 335–356). Geophysical Monograph-American Geophysical Union. https://doi.org/10.1029/GM100p0335

Leeman, W. P., Schutt, D. L., & Hughes, S. S. (2009). Thermal structure beneath the Snake River plain: Implications for the Yellowstone hotspot. *Journal of Volcanology and Geothermal Research*, *188*(1–3), 57–67. https://doi.org/10.1016/j.jvolgeores.2009.01.034

Li, C., Tao, Y., Qi, L., & Ripley, E. M. (2012). Controls on PGE fractionation in the Emeishan picrites and basalts: Constraints from integrated lithophile–siderophile elements and Sr–Nd isotopes. *Geochimica et Cosmochimica Acta*, *90*, 12–32. https://doi.org/10.1016/j.gca.2012.04.046

Libowitzky, E., & Rossman, G. R. (1996). Principles of quantitative absorbance measurements in anisotropic crystals. *Physics and Chemistry of Minerals*, *23*, 319–327. https://doi.org/10.1007/bf00199497

Lin, S. C., & van Keken, P. E. (2005). Multiple volcanic episodes of flood basalts caused by thermochemical mantle plumes. *Nature*, *436*, 250–252. https://doi.org/10.1038/nature03697

Liu, J., Xia, Q. K., Deloule, E., Ingrin, J., Chen, H., & Feng, M. (2015). Water content and oxygen isotopic composition of alkali basalts from the Taihang Mountains, China: Recycled oceanic components in the mantle source. *Journal of Petrology*, *56*, 681–702. https://doi.org/10.1093/petrology/egv013

Liu, J., Xia, Q.-K., Kuritani, T., Hanski, E., & Yu, H.-R. (2017). Mantle hydration and the role of water in the generation of large igneous provinces. *Nature Communications*, *8*, 1824. https://doi.org/10.1038/s41467-017-01940-3

Lloyd, A. S., Ferriss, E., Ruprecht, P., Hauri, E. H., Jicha, B. R., & Plank, T. (2016). An assessment of clinopyroxene as a recorder of magmatic water and magma ascent rate. *Journal of Petrology*, *57*(10), 1865–1886. https://doi.org/10.1093/petrology/egw058

Luttinen, A. V. (2018). Bilateral geochemical asymmetry in the Karoo large igneous province. *Scientific Report*, *8*, 5223. https://doi.org/10.1038/s41598-018-23661-3

Matzen, A. K., Wood, B. J., Baker, M. B., & Stolper, E. M. (2017). The roles of pyroxenite and peridotite in the mantle sources of oceanic basalts. *Nature Geoscience*, *10*(7), 530–535. https://doi.org/10.1038/ngeo2968

McDonough, W. F., & Sun, S. S. (1995). The composition of the Earth. *Chemical Geology*, *120*(3–4), 223–253. https://doi.org/10.1016/0009-2541(94)00140-4

O'Leary, J. A., Gaetani, G. A., & Hauri, E. H. (2010). The effect of tetrahedral Al3+ on the partitioning of water between clinopyroxene and silicate melt. *Earth and Planetary Science Letters*, *297*, 111–120.

Pearson, D. G., Brenker, F. E., Nestola, F., Mcneill, J., Nasdala, L., Hutchison, M. T., et al. (2014). Hydrous mantle transition zone indicated by ringwoodite included within diamond. *Nature*, *507*, 221–224. https://doi.org/10.1038/nature13080

Putirka, K. D. (2008). Thermometers and barometers for volcanic systems. *Reviews in Mineralogy and Geochemistry*, *69*(1), 61–120. https://doi.org/10.2138/rmg.2008.69.3

Ren, Z. Y., Wu, Y. D., Zhang, L., Nichols, A. R., Hong, L. B., Zhang, Y. H., et al. (2017). Primary magmas and mantle sources of Emeishan basalts constrained from major element, trace element and Pb isotope compositions of olivine-hosted melt inclusions. *Geochimica et Cosmochimica Acta*, *208*, 63–85. https://doi.org/10.1016/j.gca.2017.01.054

Salters, V. J. M., & Stracke, A. (2004). Composition of the depleted mantle. *Geochemistry, Geophysics, Geosystems*, *5*, Q05B07. https://doi.org/10.1029/2003GC000597

Shaw, D. M. (1970). Trace element fractionation during anatexis. *Geochimica et Cosmochimica Acta*, *34*, 237–243. https://doi.org/10.1016/0016-7037(70)90009-8

Shimizu, K., Komiya, T., Hirose, K., Shimizu, N., & Maruyama, S. (2001). Cr-spinel, an excellent micro-container for retaining primitive melts—Implications for a hydrous plume origin for komatiites. *Earth and Planetary Science Letters*, *189*, 177–188. https://doi.org/10.1016/s0012-821x(01)00359-4

Skogby, H., Bell, D. R., & Rossman, G. R. (1990). Hydroxide in pyroxene: Variations in the natural environment. *American Mineralogist*, *75*, 767–774.

Sobolev, A. V., Arndt, N. T., Krivolutskaya, N. A., Kuzmin, D. V., & Sobolev, S. V. (2015). The origin of gases that caused the permian-triassic extinction. *Volcanism and Global Environmental Change*, 147–163. https://doi.org/10.1007/9781107415683.011

Sobolev, A. V., Asafov, E. V., Gurenko, A. A., Arndt, N. T., Batanova, V. G., Portnyagin, M. V., et al. (2016). Komatiites reveal a hydrous Archaean deep-mantle reservoir. *Nature*, *531*, 628–632. https://doi.org/10.1038/nature17152

Sobolev, A. V., Asafov, E. V., Gurenko, A. A., Arndt, N. T., Batanova, V. G., Portnyagin, M. V., et al. (2019). Deep hydrous mantle reservoir provides evidence for crustal recycling before 3.3 billion years ago. *Nature*, *571*(7766), 555–559. https://doi.org/10.1038/s41586-019-1399-5

Sobolev, A. V., Hofmann, A. W., Kuzmin, D. V., Yaxley, G. M., Arndt, N. T., Chung, S., et al. (2007). The amount of recycled crust in sources of mantle-derived melts. *Science*, *316*, 412–417.

Sobolev, A. V., Krivolutskaya, N. A., & Kuzmin, D. V. (2009). Petrology of the parental melts and mantle sources of Siberian Trap magmatism. *Petrology*, *17*(3), 253–286. https://doi.org/10.1134/S0869591109030047

Sobolev, S. V., Sobolev, A. V., Kuzmin, D. V., Krivolutskaya, N. A., Petrunin, A. G., Arndt, N. T., et al. (2011). Linking mantle plumes, large igneous provinces and environmental catastrophes. *Nature*, *477*, 312–316. https://doi.org/10.1038/nature10385

Stefano, C. J., Mukasa, S. B., Andronikov, A., & Leeman, W. P. (2011). Water and other volatile systematics of olivine-hosted melt inclusions from the Yellowstone hotspot track. *Contributions to Mineralogy and Petrology*, *161*, 615–633. https://doi.org/10.1007/s00410-010-0553-8

Sun, S.-S., & McDonough, W. F. (1989). Chemical and isotopic systematics of oceanic basalts: Implications for mantle composition and processes. *Geological Society Special Publication*, *42*(1), 313–345. https://doi.org/10.1144/GSL.SP.1989.042.01.19

Tao, Y., Putirka, K., Hu, R., & Li, C. (2015). The magma plumbing system of the Emeishan large igneous province and its role in basaltic magma differentiation in a continental setting. *American Mineralogist*, *100*, 2509–2517. https://doi.org/10.2138/am-2015-4907

Tatsumi, Y. (2005). The subduction factory: How it operates in the evolving Earth. *Geological Society of America Today*, *15*, 4–10. https://doi.org/10.1130/1052-5173(2005)015[4:tsfhio]2.0.co;2

Taylor, H. P., & Simon, S. M. F. (1986). Igneous rocks. I. Processes of isotopic fractionation and isotope systematics. In J. W. Valley (Ed.), *Stable isotopes in high temperature processes* (pp. 227–272). Mineralogical Society of America. https://doi.org/10.1515/9781501508936-013

Thompson, D. A., Hammond, J. O. S., Kendall, J., Stuart, G. W., Helffrich, G. R., Keir, D., et al. (2015). Hydrous upwelling across the mantle transition zone beneath the afar triple junction. *Geochemistry, Geophysics, Geosystems*, *16*, 834–846. https://doi.org/10.1002/2014GC005648

Torsvik, T. H., Burke, K., Steinberger, B., Webb, S. J., & Ashwal, L. D. (2010). Diamonds sampled by plumes from the core–mantle boundary. *Nature*, *466*, 352–355. https://doi.org/10.1038/nature09216

Trela, J., Gazel, E., Sobolev, A. V., Moore, L., Bizimis, M., Jicha, B., & Batanova, V. G. (2017). The hottest lavas of the Phanerozoic and the survival of deep Archaean reservoirs. *Nature Geoscience*, *10*, 451–456. https://doi.org/10.1038/ngeo2954

Turner, M., Turner, S., Mironov, N., Portnyagin, M., & Hoernle, K. (2017). Can magmatic water contents be estimated from clinopyroxene phenocrysts in some lavas? A case study with implications for the origin of the Azores islands. *Chemical Geology*, *466*, 436–445. https://doi.org/10.1016/j.chemgeo.2017.06.032

Vinnik, L., & Farra, V. (2007). Low S velocity atop the 410-km discontinuity and mantle plumes. *Earth and Planetary Science Letters*, *262*, 398–412. https://doi.org/10.1016/j.epsl.2007.07.051

Wade, J. A., Plank, T., Hauri, E. H., Kelley, K. A., Roggensack, K., & Zimmer, M. (2008). Prediction of magmatic water contents via measurement of H_2O in clinopyroxene phenocrysts. *Geology*, *36*(10), 799–802. https://doi.org/10.1130/g24964a.1

Wan, Z., Coogan, L. A., & Canil, D. (2008). Experimental calibration of aluminum partitioning between olivine and spinel as a geothermometer. *American Mineralogist*, *93*, 1142–1147. https://doi.org/10.2138/am.2008.2758

Wang, H., van Hunen, J., & Pearson, D. G. (2015). The thinning of subcontinental lithosphere: The roles of plume impact and metasomatic weakening. *Geochemistry, Geophysics, Geosystems*, *16*, 1156–1171. https://doi.org/10.1002/2015GC005784

Xia, Q.-K., Liu, J., Liu, S.-C., Kovacs, I., Feng, M., & Dang, L. (2013). High water content in Mesozoic primitive basalts of the North China Craton and implications on the destruction of cratonic mantle lithosphere. *Earth and Planetary Science Letters*, *361*, 85–97. https://doi.org/10.1016/j.epsl.2012.11.024

Xu, R., & Liu, Y. (2016). Al-in-olivine thermometry evidence for the mantle plume origin of the Emeishan large igneous province. *Lithos*, *266*, 362–366. https://doi.org/10.1016/j.lithos.2016.10.016

Xu, Y., Chung, S., Jahn, B., & Wu, G. (2001). Petrologic and geochemical constraints on the petrogenesis of Permian–Triassic Emeishan flood basalts in southwestern China. *Lithos*, *58*, 145–168. https://doi.org/10.1016/s0024-4937(01)00055-x

Yang, Y., Ingrin, J., Xia, Q., & Liu, W. (2019). Nature of hydrogen defects in clinopyroxenes from room temperature up to 1000 C: Implication for the preservation of hydrogen in the upper mantle and impact on electrical conductivity. *American Mineralogist*, *104*(1), 79–93. https://doi.org/10.2138/am-2019-6661

Yoshino, T., Manthilake, G., Matsuzaki, T., & Katsura, T. (2008). Dry mantle transition zone inferred from the conductivity of wadsleyite and ringwoodite. *Nature*, *451*, 326–329. https://doi.org/10.1038/nature06427

Yu, H., Liu, J., Xia, Q., Gu, X., Wang, Z., & Bi, Y. (2019). Water Content of the Binchuan Picrites: Implications for the Genesis of Emeishan Large Igneous Province. *Geological Journal of China Universities*, *25*(1), 24–32. (This is a paper in Chinese).

Yu, S.-Y., Shen, N.-P., Song, X.-Y., Ripley, E. M., Li, C., & Chen, L.-M. (2017). An integrated chemical and oxygen isotopic study of primitive olivine grains in picrites from the Emeishan large igneous province, SW China: Evidence for oxygen isotope heterogeneity in mantle sources. *Geochimica et Cosmochimica Acta*, *215*, 263–276. https://doi.org/10.1016/j.gca.2017.08.007

Zhang, Z., Mahoney, J. J., Mao, J., & Wang, F. (2006). Geochemistry of picritic and associated basalt flows of the western Emeishan flood basalt province, China. *Journal of Petrology*, *47*, 1997–2019. https://doi.org/10.1093/petrology/egl034

Zhong, Y. T., He, B., Mundil, R., & Xu, Y. G. (2014). CA-TIMS zircon U–Pb dating of felsic ignimbrite from the Binchuan section: Implications for the termination age of Emeishan large igneous province. *Lithos*, *204*, 14–19. https://doi.org/10.1016/j.lithos.2014.03.005